Efficient synthesis of highly fluorescent carbon dots by microreactor method and their application in Fe 3+ ion detection

Article *in* Materials Science and Engineering C · July 2017

DOI: 10.1016/j.msec.2017.07.046

CITATIONS
0

READS
44

9 authors, including:

Long Shi Rao
South China University of Technology
6 PUBLICATIONS **3** CITATIONS
SEE PROFILE

Zongtao Li
South China University of Technology
51 PUBLICATIONS **381** CITATIONS
SEE PROFILE

Xinrui Ding
University of California, Berkeley
26 PUBLICATIONS **124** CITATIONS
SEE PROFILE

Materials Science & Engineering C 81 (2017) 213–223

Contents lists available at ScienceDirect

Materials Science & Engineering C

journal homepage: www.elsevier.com/locate/msec

Efficient synthesis of highly fluorescent carbon dots by microreactor method and their application in Fe^{3+} ion detection

Longshi Rao[a], Yong Tang[a], Zongtao Li[a,*], Xinrui Ding[b], Guanwei Liang[a], Hanguang Lu[a], Caiman Yan[a], Kairui Tang[c], Binhai Yu[a]

[a] Engineering Research Centre of Green Manufacturing for Energy-Saving and New-Energy Technology, School of Mechanical and Automotive Engineering, South China University of Technology, Guangzhou, China, 510640
[b] Department of Mechanical Engineering, University of California, Berkeley, CA 94720, USA
[c] The Mechanical Engineering, Pennsylvania State University, Harrisburg, PA 17057, USA

ARTICLE INFO

Keywords:
Carbon dots
Microreactors
Quantum yield
Ion detection

ABSTRACT

Rapidly obtaining strong photoluminescence (PL) of carbon dots with high stability is crucial in all practical applications of carbon dots, such as cell imaging and biological detection. In this study, we proposed a rapid, continuous carbon dots synthesis technique by using a microreactor method. By taking advantage of the microreactor, we were able to rapidly synthesized CDs at a large scale in less than 5 min, and a high quantum yield of 60.1% was achieved. This method is faster and more efficient than most of the previously reported methods. To explore the relationship between the microreactor structure and CDs PL properties, Fourier transform infrared spectroscopy (FTIR) and X-ray photoelectron spectroscopy (XPS) were carried out. The results show the surface functional groups and element contents influence the PL emission. Subsequent ion detection experiments indicated that CDs are very suitable for use as nanoprobes for Fe^{3+} ion detection, and the lowest detection limit for Fe^{3+} is 0.239 μM, which is superior to many other research studies. This rapid and simple synthesis method will not only aid the development of the quantum dots industrialization but also provide a powerful and portable tool for the rapid and continuous online synthesis of quantum dots supporting their application in cell imaging and safety detection.

1. Introduction

Carbon dots (CDs) are a new class of carbon nanomaterials that are regarded as a type of quantum dot with sizes below 10 nm. CDs have received steadily growing interest as a result of their peculiar and fascinating properties, such as excellent optical properties, low toxicity, good biocompatibility and robust chemical inertness [1–4]. The outstanding properties of carbon dots distinguish them from traditional fluorescent materials and make them promising candidates to replace heavy metal-based semiconductor quantum dots for numerous exciting applications, such as sensors [5], bioimaging [6], lasers [7], LEDs [8], photocatalysis [9], and photovoltaic devices [10]. Spurred by the special properties of CDs, various studies have been carried out on facile synthesis approaches and photoluminescence (PL) mechanisms. Since CDs originated from the production of carbon nanotubes by electrophoresis in 2004 [11], a broad series of methods for obtaining CDs have been developed, including pyrolysis [12], laser ablation [13], electrochemical oxidation [14], acidic oxidation [15], hydrothermal treatment [16], microwave or ultrasonic passivation [17] and plasma treatment [18]. Although remarkable successes have been achieved, the properties of these as-produced CDs, in terms of quantum yield (QY) and productivity, greatly limiting industrial applications such as in the development of photoelectric conversion devices. Beside, current synthetic methods are mainly deficient in accurately controlling the reaction conditions and continuous preparation as well as in obtaining high QYs. Therefore, it is necessary to develop a method for rapid and large scale production as well as in obtaining high QYs.

Ion pollution has become a worldwide issue due to the severe risks in organisms and environment. Up to now, a number of highly sensitive and selective methods for sensing ion or biology detection have been developed, based on quantum dots, fluorochrome, polymer materials and so on [19–23]. However, these methods generally suffer from several limitations, such as high cost, complicated operation procedures and time-consuming sample post-treatment, which greatly limit their practical application of the methods for rapid on-site analysis. Currently, the fluorescent methods have been widely employed to detect

* Corresponding author.
E-mail address: meztli@scut.edu.cn (Z. Li).

http://dx.doi.org/10.1016/j.msec.2017.07.046
Received 27 May 2017; Received in revised form 27 June 2017; Accepted 27 July 2017
Available online 30 July 2017
0928-4931/

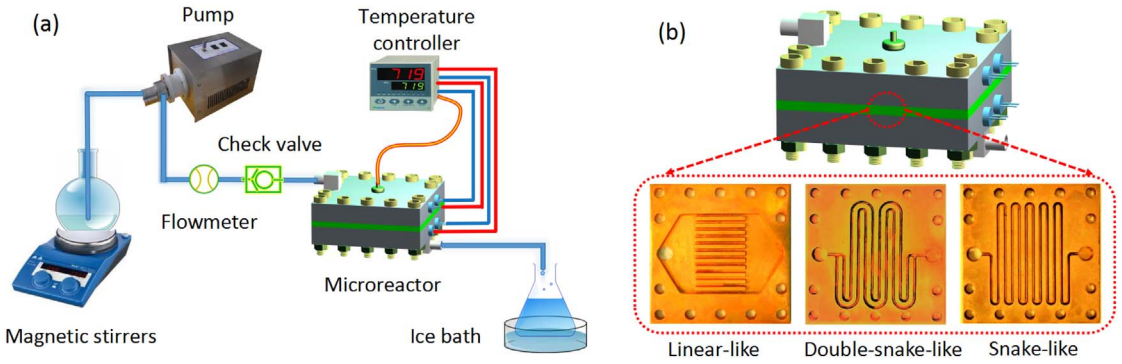

Fig. 1. (a) Diagram for the synthesis of CDs by Microreactor system. (b) Detail view of three different channels (Liaear-like, Double-snake-like, Snake-like) embed in microreactor.

targets in recent years because of their simplicity, cost-effectiveness, easy operation. The CDs has been used for ion detection due to its particular chemical and optical properties. It is well known that, a high QY is the essential factor for ion detection. However, it is still hard to rapid and efficient synthesis of CDs with high QY. In addition, it is urgent to prepare CDs online for ion detection in order to ensure measurement precision due to it is difficult to synthesize CDs using common methods outdoors or in remote areas. Therefore, it is essential to develop a powerful and portable tool for the rapid and continuous online synthesis of CDs.

In order to rapid and efficient synthesize CDs, we draw our attention to microreactors. Recently, microreactors have increasingly attracted our attention due to their advantages, including their quick heat and mass transfer properties, high speed mixing, controllable feed rates and high reproducibility [24–26]. Moreover, microreactors can provide better choices than conventional reactors for the synthesis of products that require anaerobic anhydrous environments that avoid the degradation of certain sensitive compounds. These remarkable properties have allowed their broad application in organic synthesis, nanoparticle synthesis, and medicine production [27–29]. Currently, microreactors have been regarded as a preferred method for the synthesis of high quality metal-oxides and semiconductor quantum dots [30–32]. Moreover, microreactor can not only be conveniently joined with temperature control systems or heating equipment but can also attach to analytical instruments. This enables carrying out reactions under more precisely controlled conditions than those of macroreactors. These are very important for some applications, especially in bioanalysis and safety detection.

Among reports on the use of microreactors for the synthesis of quantum dots, most of the microreactors productivity are inefficient and hardly obtain high QY. In addition, there have been few reports on the preparation of CDs using microreactors, especially less focus on the effect of microreactor structure on heat transfer. Lu et al. [33] used a microreactor with a certain length of teflon capillary tubing in oil bath to screen more than hundred of reaction conditions and investigated the relationship between different developmental stages of the CDs and their PL properties, while the QY of as-prepared CDs not more than 37%. Meanwhile, they haven't considered the effect of the inner microreactor structure on productivity and QY of CDs. Therefore, it is necessary to further explore high QY and more efficient synthesis method.

Herein, we proposed a rapid, continuous synthesized CDs method using microreactors with high efficiency. By taking advantage of the microreactor, we can rapidly synthesized CDs at a large scale in less than 5 min. Moreover, using microreactor methods, quantum yields of 60.1% and stable CDs were obtained, which is faster and more efficient than most of the previously reported methods. The relationship between the microreactor structure and the CD PL properties was also investigated, indicating inner structures have a great effect on quantum yields due to heat transfer significantly influences the synthetic process. The as-prepared CDs were used to detect Fe^{3+} ions, and the lowest detection limit (LOD) was 0.239 μM, which is superior to many other research studies. This rapid and simple synthesis method will not only aid the development of quantum dot industrialization but also provide a powerful and portable tool for the rapid and continuous online synthesis of CDs applications in bioanalysis and safety detection.

2. Materials and methods

2.1. Materials

For synthesis of carbon dots (CDs), citric acid anhydrous ($C_6H_8O_7$, ≥ 99.5%), ethylenediamine ($C_2H_8N_2$, ≥ 99.5%), and ethanol absolute (C_2H_6O, 99.5%) purchased from Aladdin have been used without further purification. Distilled water (18 MΩ) was used for all experiments.

2.2. Synthesis of CDs by microreactor method

A series of CDs was successfully synthesized by three different microreactors, as shown in Fig. 1. Typically, anhydrous citric acid and ethylene-diamine were used as precursors with deionized water as a solvent. A colourless transparent solution was prepared by dissolving anhydrous citric acid (2.25 g) in 60 ml of deionized water, followed by a few minutes of continuous stirring at room temperature. Then, additive concentrations (volumes of ethylenediamine ranging from 0.5 ml to 6.0 ml) were slowly dropped into the citric acid solution with vigorous stirring to achieve a homogeneous dispersion. Before the mixtures were injected into the microreactor, the microreactor was preheated to the rated temperature. Subsequently, distilled water was injected to clear impurities and check for gas leakages in the system. After that, when the rated temperature was achieved, the mixtures were injected by a magnetic pump with a flowmeter through a PTFE tube (inner diameter: d = 2 mm) and stainless steel tube into the linear-like microreactor. The microreactor temperatures between 80 °C and 160 °C (real temperature) were precisely controlled by a digital temperature controller. Importantly, to ensure that the flow rates (ranging from 16 ml/min to 160 ml/min) stabilized, a check valve was placed between the flowmeter and microreactor to prevent any solution and vapor from reverse flowing when the microreactor was operating at high temperatures. The samples were collected by a flask and soaked in ice water. A UV analyser with an emission maximum at 365 nm was placed on the bottom of the collection to observe the samples online. Similar procedures were also carried out for the snake-like and double-snake-like microreactors depending on the variation of the reaction temperature, additive concentration and flow rate.

2.3. Metal ion detection

For the detection of metal ions, various metal ion solutions,

including Fe^{3+}, Co^{2+}, Cr^{3+}, Cu^{2+}, Fe^{2+}, Pb^{2+}, Mn^{2+}, Ca^{2+}, Cd^{2+} and Zn^{2+}, were used to detect the fluorescence intensity of the CDs. The aforementioned ion solution was prepared from reagents containing Cl^- ions with a concentration of 50 μM and pH of 7. After, 0.5 ml of CDs were added into 3 ml of the ion solution and allowed to react for 1 min under light stirring to form a homogeneous solution. To evaluate the CD sensitivity towards Fe^{3+}, a series of concentrations (ranging from 0 to 1 mM) of Fe^{3+} were added into the aqueous solution containing the same number of CDs. The PL spectra of the CDs in the absence and presence of various metal ions were measured by a 365 nm excitation source. All experiments were conducted at room temperature.

2.4. Measurement

The surface morphology of the CDs was characterized by transmission electron microscope (TEM, JEM-2100F, JEOL, Japan) with an accelerating voltage of 200 kV. The phase purity and structure of the as-prepared CDs were measured using an X-ray diffractometer (XRD, D8-Advance, Bruker, Germany) with a Cu-Kα radiation source (λ = 0.15418 nm) at a counting rate of 0.02° per minute in the scanning angle (2θ) range from 5° to 80°. The X-ray photoelectron spectroscopy (XPS) data were collected by an X-ray photoelectron spectrometer (Kratos Axis Ulra DLD, Kratos, UK) with a mono Al-Kα excitation source (1486.6 eV). Fourier transform infrared (FTIR) spectra were recorded from 4000 to 400 cm^{-1} on an FTIR spectrometer (VERTEX 33, Bruker, Germany) in KBr discs after being vacuum-dried for 12 h. The ultraviolet visible (UV–vis) absorption spectra were measured by using a UV–vis spectrometer (UV–vis, Shimadzu, Japan). The excitation and emission spectra of the CDs were recorded using a fluorescence spectrophotometer (RF-6000, Shimadzu, Japan) with a Xe lamp as an excitation source. The quantum yield (QY) of the CDs was calculated by the following equation [34].

$$Q_X = Q_{ST}\frac{Grad_X}{Grad_{ST}}\cdot\frac{\eta_X^2}{\eta_{ST}^2} \quad (1)$$

where the Q is the QY and the subscripts X and ST denote test and standard, respectively; quinine sulfate dissolved in 0.1 M H_2SO_4 (QY 0.54 at 365 nm) was used as the standard. Grad represents the slope determined by the ratio of the linear curves of the integrated fluorescence intensity to UV–vis absorbance (λ = 365 nm). η is the refractive index of the solvent. The integrated emission intensity is the area under the photoluminescence curve in the wavelength range of 380–700 nm. The graphs plotted the integrated emission intensity against the absorbance. Meanwhile, the standards were chosen to ensure they absorbed at the excitation wavelength of choice for the test samples. To reduce reabsorption effects, the absorbance of the standard and test samples at and above the excitation wavelength did not exceed 0.1. Solutions with five different concentrations of the chosen standard and test sample minimized the experiment error.

3. Results and discussion

Compared to conventional methods for preparing CDs, the microreactor method has an advantageous reaction rate, product yield, and so on. To illuminate the utility of the microreactor for quick synthesis of CDs, different flow rates were selected. The reaction temperature is 160 °C and the amount of ethylenediamine is 1 ml. The calculated reaction times of each flow rate are given in Table 1. As depicted in Table 1, the difference of the total reaction time between flow rates of 16 ml/min and 80 ml/min is approximately 2 min. When the flow rate is more than 80 ml/min, the difference between the total reaction times is approximately 0.5 min. In a word, all of the total reaction time are less than 5 min.

UV–vis absorption spectra were obtained to characterize the effect of the flow rate on the CD properties, as shown in Fig. 2(a)–(c). Generally, all the samples show that the flow rate greatly influenced the UV–vis absorption spectra of the corresponding CDs. Interestingly, the CDs prepared by different microreactor designs exhibit very a similar variation tendency in their UV–vis absorption spectra. That is, as the flow rates increase, the UV–vis characteristic absorption peak intensities decrease. As shown in Fig. 2(a)–(c), when the flow rates range from 16 ml/min to 160 ml/min, all of the absorption peak intensity decline and have slight blue shifts. This phenomenon may be related to the concentration and size decrease of the CDs. Moreover, among the three different microreactors, the absorption peak intensity of the linear-like microreactor was larger than others at the same flow rate, owing to the more sufficient mixing reaction in the linear-like microreactor.

Table 1
Reaction time of different flow rate.

Flow rate/(ml/min)	16	40	80	120	160
Total reaction time/min	4.56	3.43	2.61	2.12	1.66

In addition, the PL of the CDs was also investigated to further elucidate the effect of flow rates on the CD properties, as shown in Fig. 3(a)–(c). When the flow rates increase, the PL intensities decrease. The flow rate affects the residence time. For the microreactor system, the residence time in the microreactor has an effect on the properties of the CDs. When the flow rate is fast, the residence time is short for the same channel. As a consequence, the PL intensity decreases, as demonstrated in Fig. 3(a)–(c). However, the residence time is determined not only by flow rate but also by the microreactor channel length. Among the three different microreactors, the snake-like microreactor has the longest channel length. This means the CDs synthesized by the snake-like microreactor have a long residence time and thus result in a bigger size. This result is further confirmed by TEM. Although channel length affects the reaction residence time, the process synthesis of CDs is complicated and is significantly influenced by a number of factors, such as the reaction temperature, additive concentration and pressure. This is why the snake-like microreactor with the longest channel length does not result in the strongest PL intensity. To further explore the factors involved in preparing CDs, the reaction temperature and additive concentration were investigated, and the screening procedure study is detailed in the supporting information. The UV–vis spectra and PL spectra of the CDs were also obtained to screen the reaction conditions, as shown in Figs. S1–S2 and Figs. S3–S4, respectively. According to the results, we found that the additive concentration and reaction temperature have important effects on the UV–vis spectra and PL spectra of the corresponding of CDs. When the additive concentration ranges from 0.5 ml to 6.0 ml, the entire UV–vis absorption band from 800 to 220 nm increases gradually and the absorption peak is at approximately 350 nm. Moreover, the absorption peak is most obvious when the additive concentration is 1.5 ml. This phenomenon indicates that the optimized additive concentration reduces CD surface defects and enhances photoluminescence. This point is further confirmed by the PL spectra (Fig. S3). The reaction temperature influences the carbonization extent. As the reaction temperatures increase, both the intensity of first absorption peak and PL increase. Moreover, at the same CDs concentration, the CDs were synthesized by the linear-like microreactor with a high PL intensity (Figs. S3–S4). This phenomenon may be closely related to the uniformity of the heated solution. Therefore, it is necessary to achieve optimized conditions to obtain high quantum yields.

The reaction conditions can be screened quickly and effectively by using the microreactor system (shorter than 5 min). The optimized conditions of the additive precursor concentration, reaction temperature, and flow rate are 1.5 ml, 160 °C and 16 ml/min for the three different microreactors, respectively. Fig. 4(a)–(c) shows the UV–vis

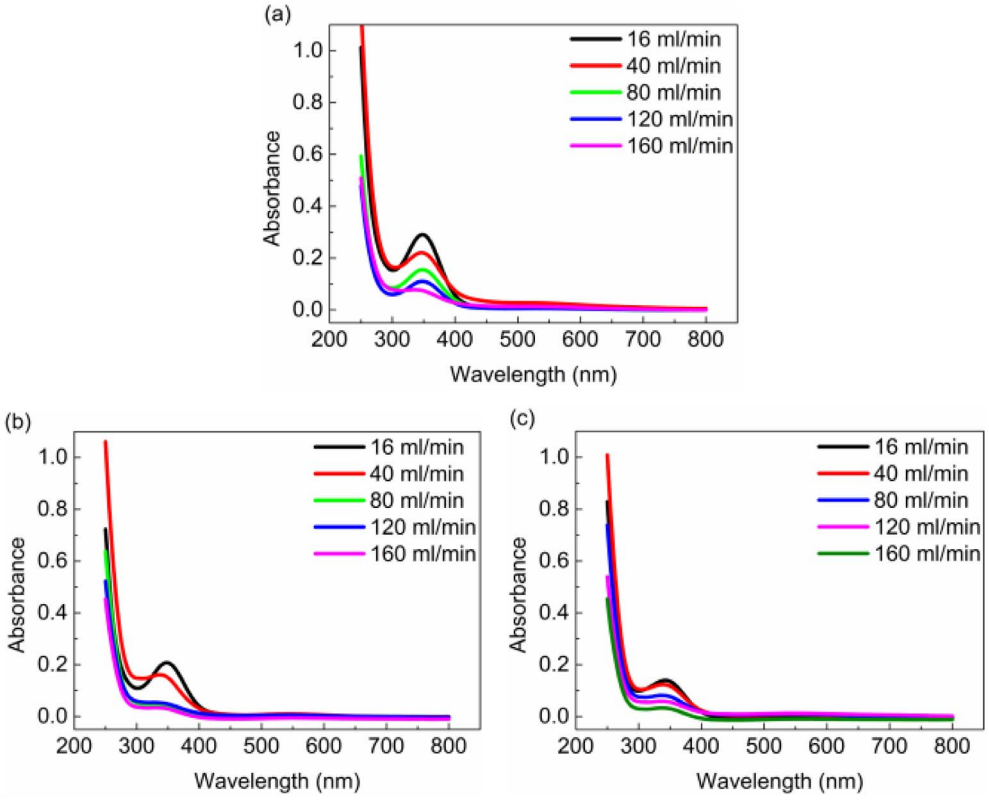

Fig. 2. UV–vis spectra of CDs obtained by three different microreactors: (a) linear-like microreactor, (b) snake-like microreactor, and (c) double-snake-like microreactor with different flow rates.

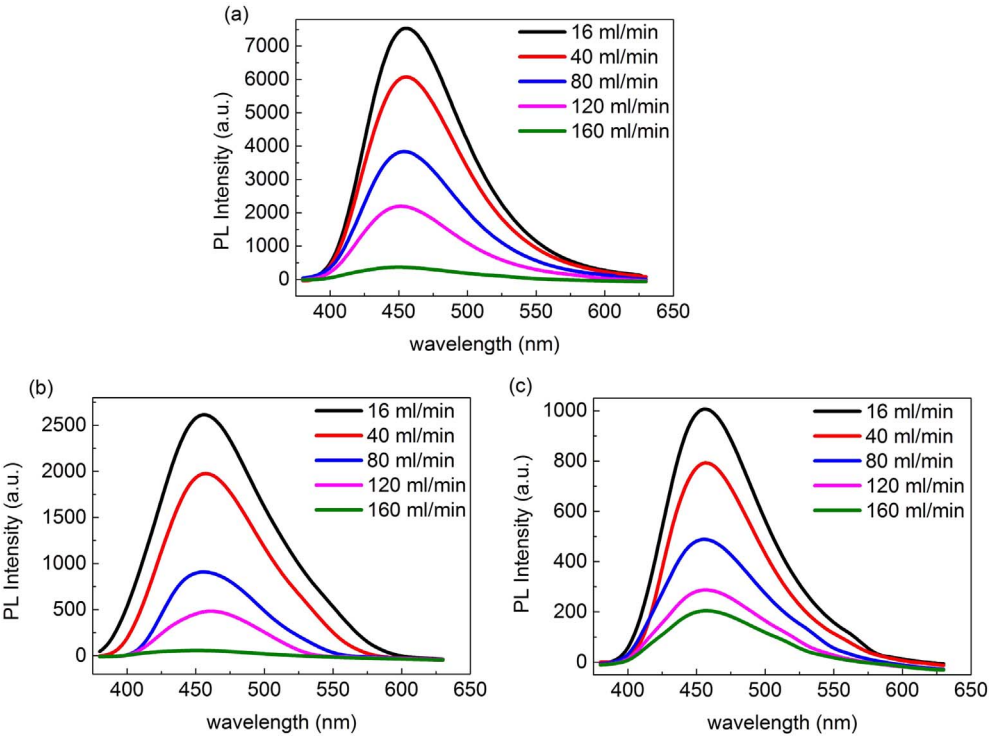

Fig. 3. PL spectra of CDs obtained by three different microreactors: (a) linear-like microreactor, (b) snake-like microreactor, and (c) double-snake-like microreactor with different flow rates.

absorption spectra and PL spectra of the optimized conditions of the CDs that were synthesized by the linear-like, double-snake-like and snake-like microreactors, namely, L-CDs, DS-CDs and S-CDs, respectively. The inset images show the bright colour of the solution under sunlight radiation and under a UV analyser (365 nm exciting source) radiation, indicating the formation of fluorescent carbon quantum dots. Moreover, all of the CDs show strong absorption at approximately 350 nm, with a tail extending to the visible range. At wavelengths below 300 nm, other absorption peaks were not observed. This result indicates that the samples are of high purity. The absorption peak located at 350 nm represents the typical absorption of an aromatic π system (n–π* transition) or other connected surface functional groups [8]. The surface functional groups including oxygen functional groups and nitrogen functional groups usually easily attach on the surface of

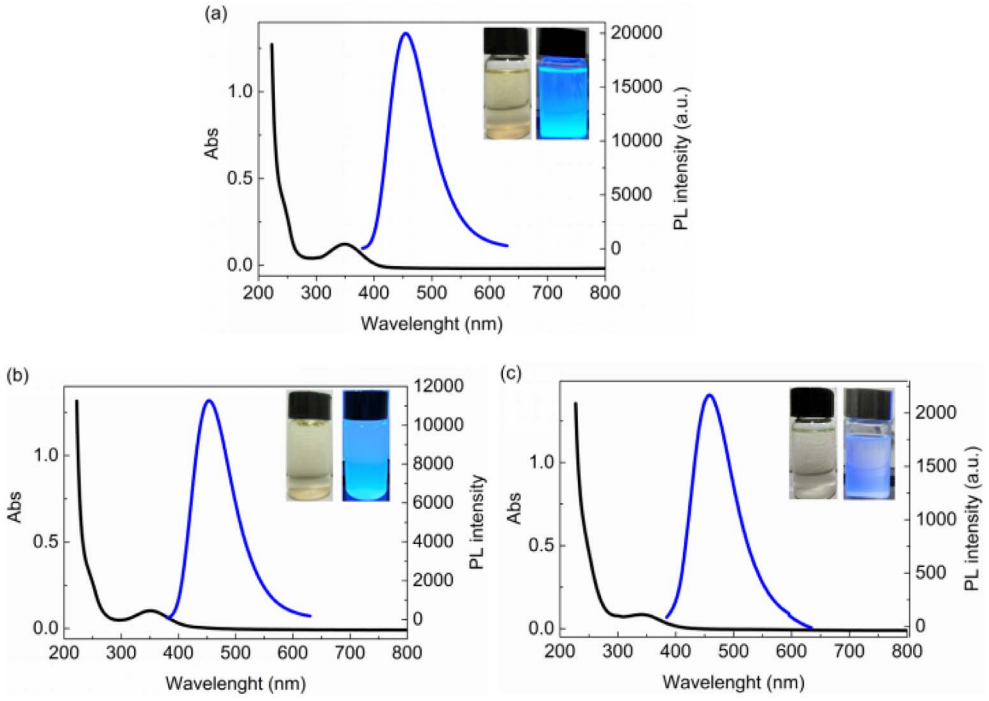

Fig. 4. UV–vis absorption spectra and PL spectra of CDs obtained by three different microreactors: (a) linear-like microreactor, (b) snake-like microreactor, and (c) double-snake-like microreactor (insets are under sunlight radiation and ultraviolet radiation at 365 nm).

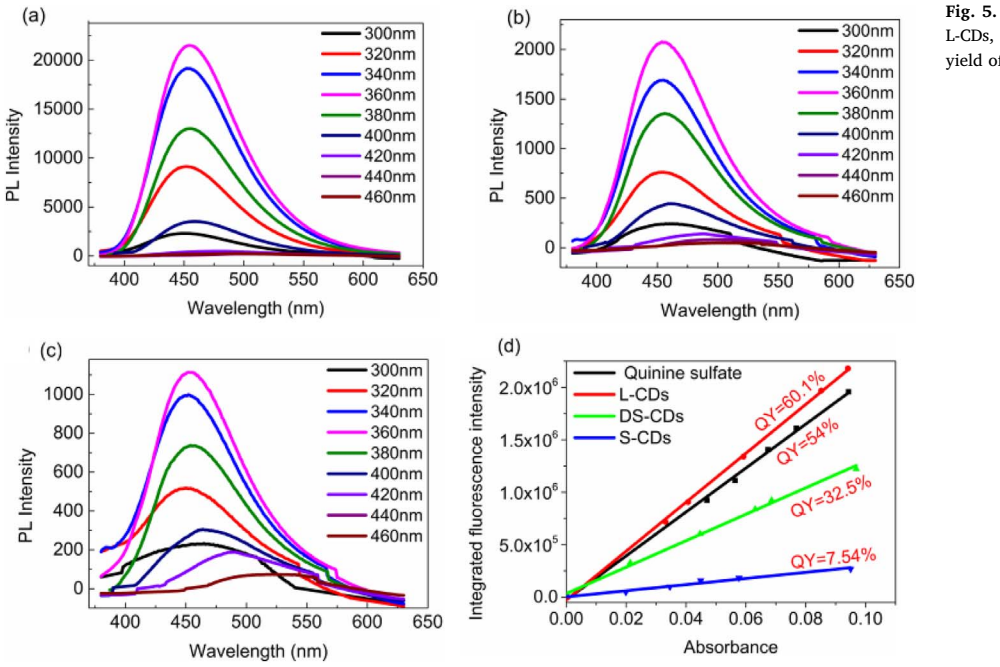

Fig. 5. (a)–(c) The excitation-dependent PL spectra of the L-CDs, DS-CDs and S-CD, respectively. (d) The quantum yield of the L-CDs, DS-CDs and S-CD.

CDs during the synthesis process; these groups play an important role in originating the fluorescence under the illumination of UV-light at a specific wavelength [35–37]. Meanwhile, the absorption peak intensities of CDs prepared by the three different microreactors differ slightly. The absorption deviations for the three types of CDs represent, at least to some extent, the different surface functional group structures or surface states of the CDs.

The PL spectra of the CDs are investigated in Fig. 4(a)–(c), showing that the emission peak of the CDs is wide compared to other semiconductor quantum dots (QDs). The full width at half maximum (FWHM) values of the luminescent peak of L-CDs, DS-CDs and S-CDs are 78 nm, 81 nm and 87 nm, respectively. This is one of the main differences between CDs and QDs. Moreover, the emission peak position of the CDs depends on the excitation wavelength, as shown in Fig. 5(a)–(c). The PL spectra reveal a strong emission peak at 455 nm with an excitation of 365 nm. Interestingly, the observed excitation-dependent emission luminescence properties are similar to those reported previously [38,39]. The maximum emission red shifts (Fig. S5) when increasing the excitation wavelength. This phenomenon may be related to the surface state, molecular state or other salvation effects. The excitation-dependent character can be further applied in displays, cell imaging and other applications.

Moreover, based on the optimal conditions, the quantum yield (QY) was measured with quinine sulfate as a standard (QY = 54%), as shown in Fig. 5(d). The quantum yield of the L-CDs, DS-CDs and S-CDs is 60.1%, 32.5% and 7.54%, respectively. The QY reaches up to 60.1%

Table 2
The comparison of different synthesis methods of carbon dots.

Methods	Precursors	Reaction time	Other conditions	Quantum yield	Refs
Hydrothermal method	Citric acid, ethylenediamine	5 h	150–300 °C	80.6%	[48]
	Citric acid, L-cysteine	3 h	200 °C	73%	[49]
	Sodium citrate, NH_4HCO_3	4 h	180 °C	68%	[50]
Arc-discharge	Carbon soot	48 h	HNO_3, boiled	1.6%	[11]
Laser ablation	Carbon soot	72 h	PEG_{1500N}, 120 °C	4–10%	[13]
Microwave pyrolysis	Saccharide, PEG	2–10 min	500 W	3.1–6.3%	[51]
	Glucose, amino acids	35 min	125 °C and 275 °C	30–69%	[52]
Ultrasonic synthesis	Glucose	4 h	HCl or NaOH	7%	[53]
Thermal pyrolysis	Citric acid, diethylenetriamine	30 min	170 °C	88.6%	[54]
Microreactor method	Citric acid, ethylenediamine	1.66–5 min	160 °C	60.1%	This work

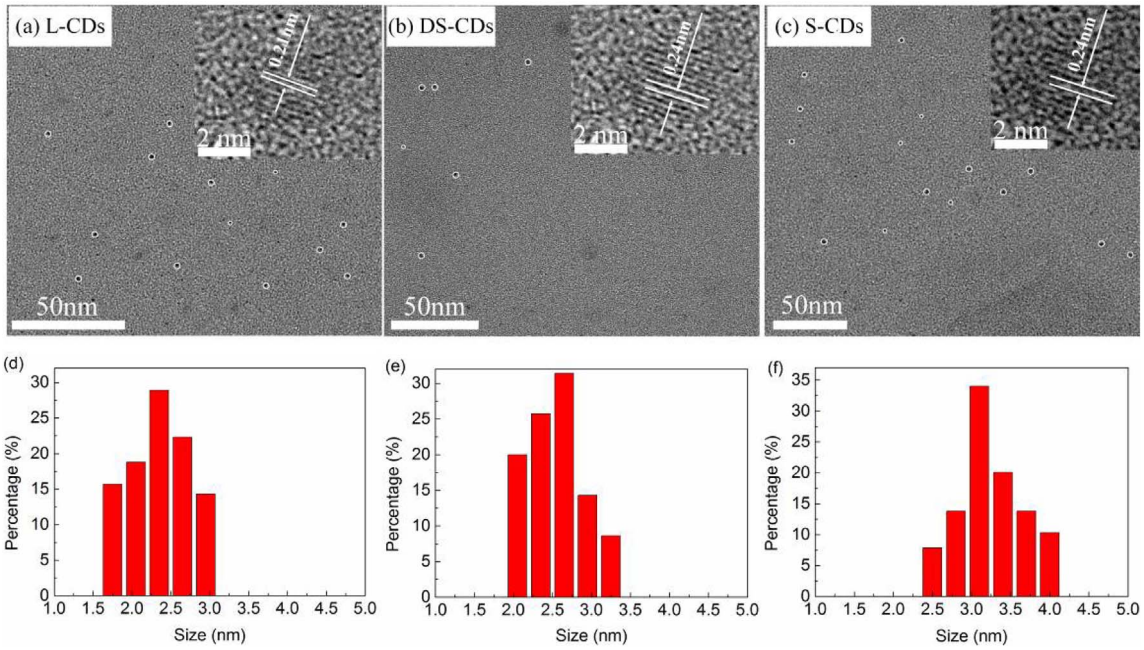

Fig. 6. (a)–(c) TEM images of the L-CDs, DS-CDs and S-CDs, respectively (insets are HRTEM images); (d)–(f) The size distribution histograms of the L-CDs, DS-CDs and S-CDs, respectively.

when using the linear-like microreactor, which is higher than the QY values previously reported for CDs [40]. The L-CDs have a high emission intensity and QY, possibly owing to uniform heating and reaction rates.

Under the optimum reaction conditions, the total reaction times are not more than 5 min (60 ml solution). These are much faster than most of the rates previously reported at the same scale, as shown in Table 2. In addition, this new device not only has obvious merits in efficiency but also obvious merits in scale. Meanwhile, the quantum yield of the as-prepared CDs is also comparable to that of the CDs obtained by the hydrothermal approach at high temperatures. All these results indicate that microreactors are advantageous for high reaction rates, lager scales and high quantum yields.

The synthesis of CDs by using microreactor methods is a complex chemical process, and it is hard to determine the exact reaction mechanism. To further explore the potential of the reaction mechanism of CDs in a microreactor system, various characterizations of the as-prepared CDs, such as TEM, XRD, FTIR, XPS, were carried out.

The surface morphology of as-prepared CDs was characterized by transmission electron microscopy, (TEM) presented in Fig. 6(a)–(c). The results reveal that the as-prepared CDs are well dispersed without aggregation and mostly spherical in shape with an average diameter of approximately 2.40 nm, 2.58 nm, and 3.23 nm for the L-CDs, DS-CDs and S-CDs, respectively. The high resolution TEM (HRTEM) images provided in the inset show CDs with lattice spacing distances of 0.21, 0.24 and 0.24 nm, which are consistent with the (100) facet of graphitic carbon [41]. Meanwhile, most CD nanoparticles possess amorphous structures, which is different from the previous reports suggesting that the CDs are composed of multicrystalline and amorphous carbon [42]. The size distribution histograms of these CDs are shown in Fig. 6(d)–(f).

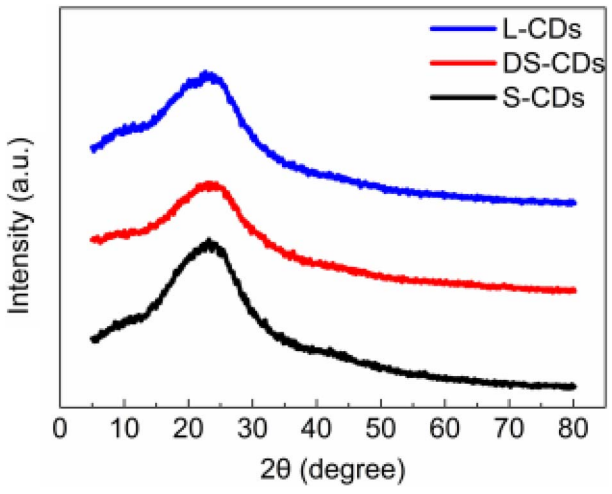

Fig. 7. XRD patterns of the L-CDs, DS-CDs and S-CDs, respectively.

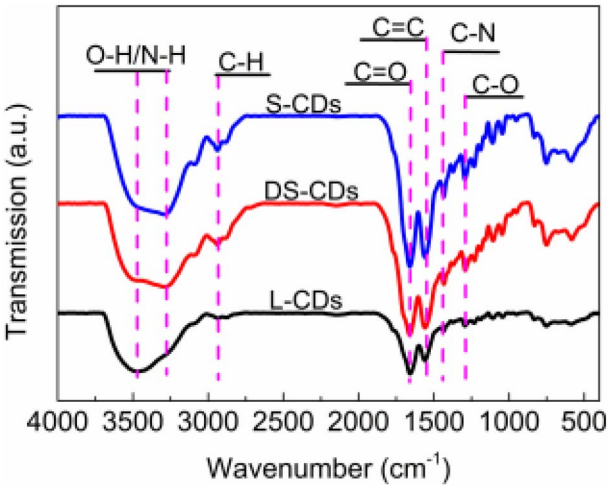

Fig. 8. FTIR spectra of the L-CDs, DS-CDs and S-CDs, respectively.

The S-CDs that were synthesized via the snake-like microreactor exhibit larger grain diameters than the others, and the particle size distribution is broader than the others. This phenomenon indicates that the shape of the channel will affect the growth of the crystal. The snake-like microreactor with the single and longest channel gave the mixture a longer reaction time, which is good for crystal growth. However, too long of a reaction time will not be propitious for the formation of uniform particles. This point is proved by Fig. 6(f), showing a broad particle size distribution. Moreover, we did not find the same phenomenon as many semiconductor quantum dots that show size-dependent PL emission. This suggests that the PL colour does not change with the size of the CDs, and the PL intensity of the CDs is relative to the surface groups or other surface states rather than the size. This is another main difference between CDs and QDs.

The XRD diffractogram of the three types of CDs is shown in Fig. 7. Each of them has a similar and broad single diffraction peak at 23.3°, 23.5° and 23.6°, respectively. Meanwhile, no impurity peaks were observed, confirming the high purity of the three products. In addition, the XRD pattern demonstrate an obvious peak width at half height (FWHM) difference among the three types of CDs, and the FWHM of the

Table 3
The atomic percentages and the corresponding C1, N1 s and O1s peaks of the centre binding energy of three different CDs.

Sample	C atomic percentages	N atomic percentages	O atomic percentages
L-CDs	72.95%	8.41%	18.64%
SS-CDs	78.79%	8.52%	12.69%
S-CDs	82.62%	5.08%	12.30%

L-CDs is bigger than others, which means that S-CDs have a smaller size diameter. This consequence is consistent with TEM analysis. Otherwise, the XRD pattern displays the highly disordered amorphous carbon of CDs. All these XRD and TEM results confirmed that the three types of CDs have a graphitic structure.

However, we cannot determine why the PL variation occurs among the three types of CDs just using the above characterization analysis. Therefore, to further explore the possible causes, Fourier transform infrared (FTIR) and X-ray photoelectron spectroscopy (XPS) were carried out in order to explore the chemical composition and the chemical bonding of the CDs.

FTIR was carried out to characterize the composition of as-prepared CD groups, as shown in Fig. 8. The FTIR spectra of the L-CDs, SS-CDs and S-CDs synthesized via various microreactors are similar except for the relative intensity of certain bands that vary and indicate special character. The broad absorption peak at 3450–3280 cm^{-1} was ascribed to the stretching vibrations of O—H and N—H, which means the formation of –OH occurs during the synthesis of the three different CDs. The absorption peak located at approximately 2930 cm^{-1} suggests stretching vibrations of $-CH_2$. Moreover, stretching vibrations of the C═O (1650 cm^{-1}), C═C (1557 cm^{-1}), C-N = (1445 cm^{-1}), and C—O (1285 cm^{-1}) bands were observed for each CD, indicating the formation of polyaromatic structures in the three different CDs during the synthesis process [43]. The band at approximately 1250–1650 cm^{-1} was ascribed to the skeletal vibrations of the aromatic rings. Careful comparisons between the different CDs.

FTIR spectra revealed some important observations. First the broad absorption peak centre position of the typical stretching vibrations of O—H and N—H bonds shifts from 3450 to 3280 cm^{-1} corresponding to the carbon type changes from L-CDs to S-CDs. This result indicates an

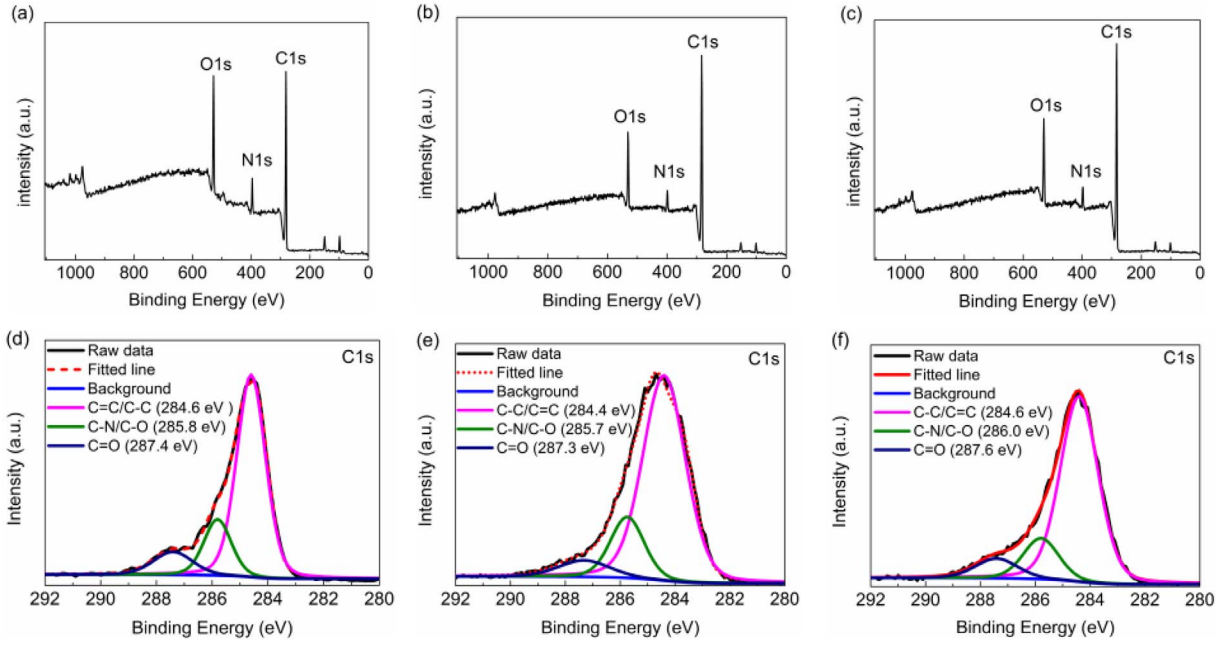

Fig. 9. (a)–(c) XPS spectra of the L-CDs, DS-CDs and S-CDs, respectively; (d)–(f) High resolution of C1s peaks of the L-CDs, DS-CDs and S-CDs, respectively.

Table 4
XPS data analysis of the C1s spectra of three types of CDs.

Sample	C═C/C−C	C−N/C−O	C═O
L-CDs	70.58%	18.60%	10.82%
SS-CDs	75.28%	17.60%	7.12%
S-CDs	75.55%	15.57%	8.88%

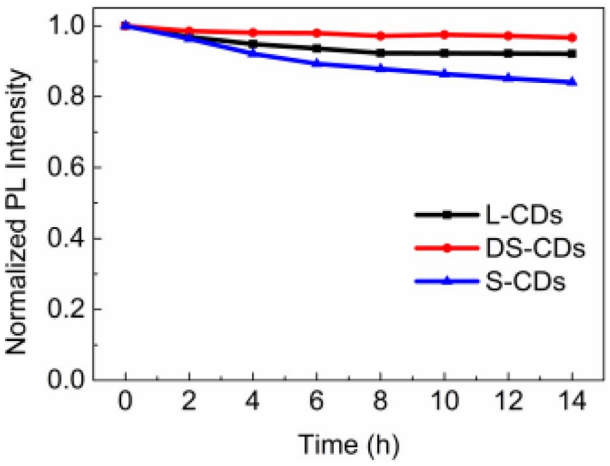

Fig. 10. The photostability of the three types of CDs under different ultraviolet lamp irradiation times.

increase in the degree of amidogen modification on the surface of CDs. Second, the $-CH_2$ vibration bands around at 2930 cm^{-1} become more and more sharp when the carbon type changes from L-CDs to S-CDs. The final and most important observation is the absorption peak in the fingerprint region (1000–400 cm^{-1}) that is complicated and includes C−O, C−H, N−H and O−H differences existed in the FTIR spectra of the different CD structures that have hardly been observed; thus, it necessary to conduct other characteristic analyses to further explore the forming mechanism. According to the analyses, we can draw that conclusion that the content of the surface functional groups and elements leads to different PL intensities between the three types of CDs. XPS was employed to characterize the element content and configuration of the surface groups of the three different CDs.

The XPS survey spectra for the CDs are shown in Fig. 9(a)–(f). They indicate that all of the CDs consist of carbon (C), nitrogen (N) and oxygen (O), and the atomic percentages and the corresponding C1, N1s and O1s centre peaks of three different CDs are depicted in Table 3. In Table 3, the content of the carbon atom in the CDs increases from

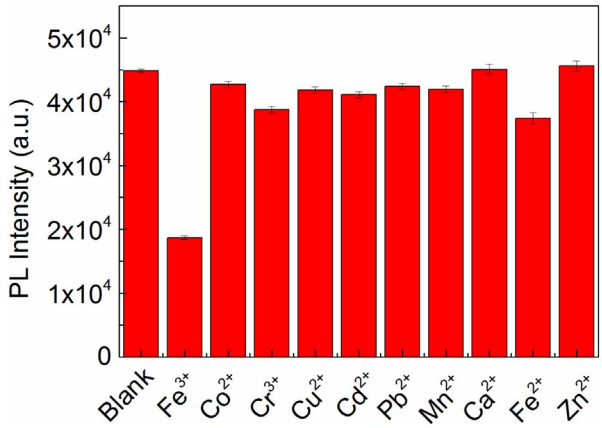

Fig. 12. Comparison of PL intensities of CDs after adding different metal ions.

sample L-CDs to S-CDs. This suggests that the channel length (meanly residence time increase) increase will improve crystal growth. This result supports the XRD and TEM analyses indicating that residence time increase greatly affects crystallization. All of the high-resolution CD spectra contain a C1s band that can be divided into three peaks corresponding to the sp^2 carbon (C−C/C═C), sp^3 carbons (C−O/C−N) and carbonyl carbons (C═O), respectively [44]. Moreover, the XPS intensity of C1s at 284.6 eV gradually increases from sample L-CDs to S-CDs, implying a corresponding increase in the content of the sp^2 carbon (C−C/C═C) groups in the CDs (Table 4), consistent with the FTIR results. The above XPS spectroscopic analysis agrees well with the FTIR results, further verifying the existence of surface groups in the CDs and the relationship between the microreactor shape and product. What is more, it is found from Tables 3 and 4 that higher N or O element contents are good for creating a high PL intensity. The FTIR and XPS analyses demonstrate that three different CDs contain abundant surface functional groups (C−C, C−O, N−H, −OH, etc.), implying unexceptionable water solubility without needing further passivation, which has great potential applications in bioscience and food safety detection.

The photostability of the CDs was investigated under different incandescent lamp exposure times, as shown in Fig. 10. The CDs were exposed under the ultraviolet lamp (10 W) for 14 h. After 14 h, the PL intensity of the L-CDs, DS-CDs and S-CDs decreased 7.88%, 3.37% and 15.93%, respectively. The result indicates that all of CDs possess good photostability, which benefit from the carbon core-based PL centre [45]. Moreover, DS-CDs have the best photostability among the three different CDs, which may be related to the quantity and content of its functional groups. Moreover, no blinking was observed in the three types of CDs when undergoing continuous high power UV exposure. These photostability data signify that the CDs have an immense

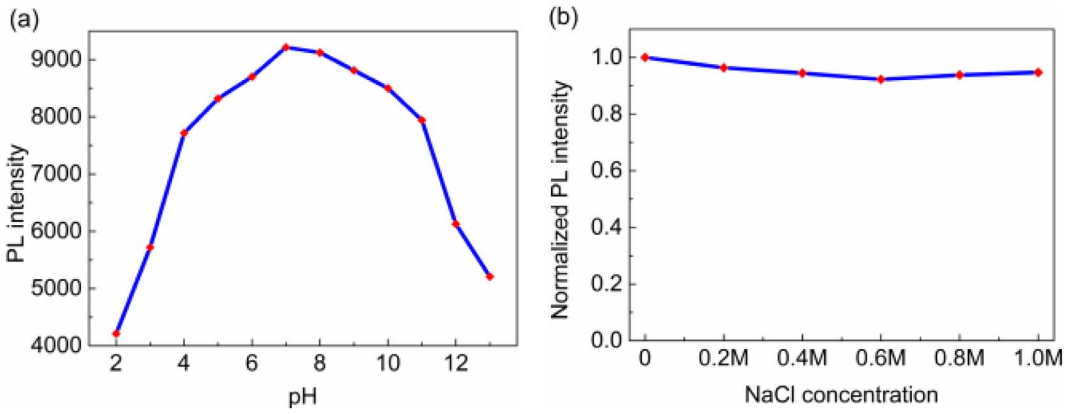

Fig. 11. The photostability of the three types of CDs under different (a) pH values and (b) NaCl concentrations.

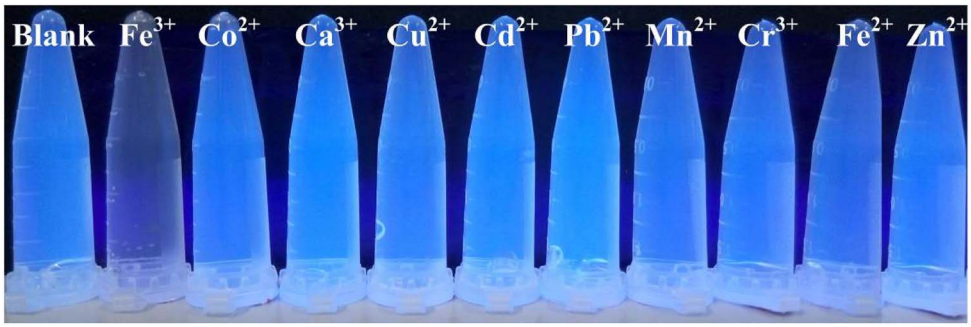

Fig. 13. The PL intensities of CDs after adding different metal ions under 365 nm UV light irradiation.

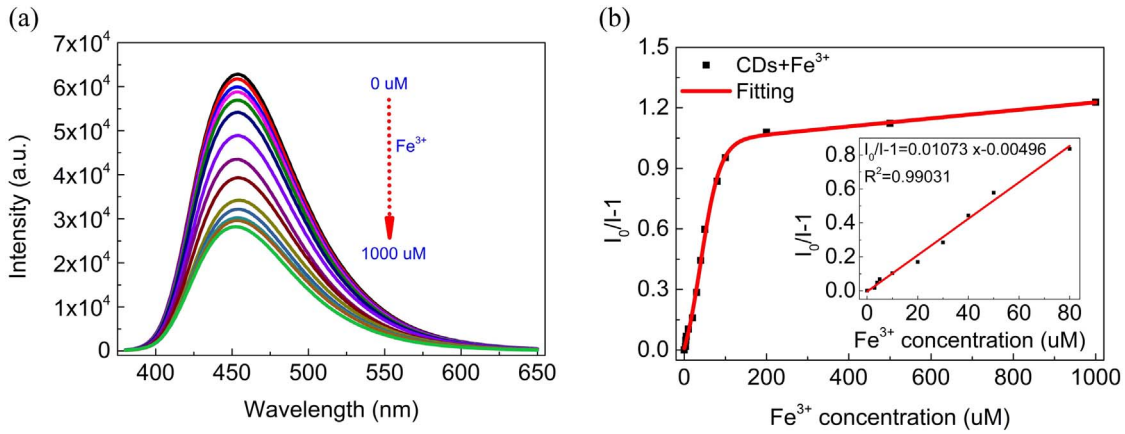

Fig. 14. (a) PL emission spectra of the CDs in the presence of various concentrations of Fe^{3+}. (b) Stern-Volmer plot as a function of Fe^{3+} concentration.

potential application value.

Furthermore, pH and salt concentration stability is also essential to CDs that are usually used for bioimaging and analytical detection. Therefore, the stability of the DS-CDs was investigated under different pH values and ionic strengths, as shown in Fig. 11 (a)–(b). When the pH varies from 5 to 10, the PL intensities (Fig. 11(a)) of the DS-CDs exhibit nearly no obvious decrease and the largest response at pH 7, which is suitable for applications involving in vivo environments. In addition, at different NaCl concentrations (Fig. 11(b)), the PL intensities show no remarkable changes, which suggests that the DS-CDs are available for bioscience studies in various physical salt concentrations. PL intensity versus time and temperature as shown in Fig. S6 (a)–(b). All these results show that CDs have a great stability.

To examine the CDs properties for safe detection, we explored the feasibility of CDs as a nanoprobe for the detection of representative metal ions. The influence of metal ions on the fluorescence intensity of the CDs was investigated by comparing the fluorescence intensity in the presence and absence of various metal ions. As shown in Fig. 12, no obvious PL changes were observed in the presence of the other metal ions (Co^{2+}, Cr^{3+}, Cu^{2+}, Fe^{2+}, Pb^{2+}, Mn^{2+}, Ca^{2+}, Cd^{2+}, Zn^{2+}) expect for Fe^{3+}, implying that it is possible for CDs to be used as a nanosensing platform for Fe^{3+} ion detection. The mechanism of fluorescence quenching of CDs with Fe^{3+} might be related to the interaction between Fe^{3+} and oxygen-containing groups on the CD surface, which leads to a metal-quenching effect [46]. The photographs of CDs in the presence and absence of metal ions under 365 nm UV light irradiation are shown in Fig. 13.

For further sensitivity studies, different concentration of Fe^{3+} were added to aqueous solutions containing the same number of CDs to evaluate the detection ability of Fe^{3+}. As shown in Fig. 14(a), the fluorescence intensity of the CDs at approximately 455 nm gradually declines along with the increase of the Fe^{3+} concentration range from 0 to 1000 μM, suggesting that this system is sensitive to Fe^{3+} ions. The fluorescence quenching data follow the Stern-Volmer equation:

$$I_0/I = 1 + K[C] \quad (2)$$

where I_0 and I are the fluorescence intensities of the CDs at 455 nm in the absence and presence of the Fe^{3+} ions solution, respectively. The variable K is the Stern-Volmer quenching constant, and [C] is the concentration of Fe^{3+}. A good linear correlation (R^2 = 0.9903) was observed over the concentration range of 0–80 μM (Fig. 14(b)). The lowest detection limit (LOD) was calculated to be 0.239 μM at a signal-to-noise ratio of 3 based on the standard deviation (SD) of 10 blank measurements and the slope (S) of the calibration curve at levels approximating the LOD, according to the formula: LOD = 3.0 (SD/S) [47]. The detection sensitivity of Fe^{3+} is superior to some previously reported studies (Table 5). The above analysis clearly confirmed that CDs can be used as a nanoprobe with high efficiency for Fe^{3+} detection.

To test the practicability of CDs based nanosensing platform, we extended it to determine the concentration of Fe^{3+} in real water samples from the ZhuJiang river. The samples were centrifuged at 10000 rpm for three times and then the supernatant liquid was filtered

Table 5
Comparison of the sensing performance of different fluorescent probes for Fe^{3+} detection.

Fluorescence probes	Detection limit (μM)	Linear range (μM)	Refs
Carbon dots	2.9	0–250	[55]
Carbon dots	0.7	5–80	[56]
Carbon dots	0.5	5–100	[57]
Carbon dots	1.3	2–50	[58]
N-Carbon dots	4.67	5–1280	[59]
P-Carbon dots	0.005	0–20	[60]
N-Carbon dots	0.025	0.1–500	[61]
Carbon dots	0.239	0–80	This work

Table 6
Detection of spiked Fe^{3+} in water samples (n = 3, pH = 7.0) using the CDs based nanosensing platform.

Sample	Spiked (μM)	Found by this work (μM)	Recovery ± RSD (%, n = 3)
1	10	10.18	102.56 ± 1.3
2	20	20.22	101. 12 ± 1.8
3	30	31.12	102.43 ± 1.6

by using filter membranes. A recovery experiment was carried out with Fe^{3+} of different concentrations to the water samples. The PL intensity of CDs decreased when the samples were spiked with Fe^{3+} standard solutions. As shown in Table 6, the found values were consistent with the addition of Fe^{3+}. The recoveries were in the range 101.12–102.56% and the relative standard deviations (R.S.D.) of three replicate detections for each sample were below 5%. These results proved indicated the potential promise of the photoluminescent CDs in the practical applications.

4. Conclusions

In conclusion, we proposed a rapid, continuous CD synthesis technique using three different microreactors. The additive concentration, reaction temperature, and flow rate were quickly screened, and the optimal conditions are 1.5 ml, 160 °C and 16 ml/min, respectively. By taking advantage of the microreactor, we can rapidly synthesize CDs in less than 5 min; this method is faster than most of those previously reported. Moreover, a high quantum yield of 60.1% was achieved by using a linear-like microreactor, and this yield is comparable to or greater than that of the common hydrothermal approach. The relationship between the PL emission and different microreactor-synthesized CDs was investigated. The results show that the surface functional groups and the element content influence the PL emission, especially nitrogen and oxygen-containing functional groups. Besides, the PL intensity of CDs arises predominantly from their surface states, rather than from their size. The PL stability of CDs was also investigated under different incandescent lamp exposure times, pH values and NaCl concentrations, revealing CDs with a good stability. Further experiments demonstrated that CDs are very suitable to be used as nanoprobes for Fe^{3+} ion detection. This study fully illuminates that the microreactor synthesis system is not only a promising tool for rapid, continuous CD synthesis but also a significantly valuable tool for cell imaging and ion detection.

Acknowledgements

This work was financially supported by the National Natural Science Foundation of China (U1401249 and 51405161), the Science & Technology Program of Guangdong Province (2014B010121002), the Natural Science Foundation of Guangdong Province, (2014A30312017), and the Science & Technology Program of Guangdong Province, (2015B010114003).

Appendix A. Supplementary data

Supplementary data to this article can be found online at http://dx.doi.org/10.1016/j.msec.2017.07.046.

References

[1] J. Zhang, S.-H. Yu, Carbon dots: large-scale synthesis, sensing and bioimaging, Mater. Today 19 (2016) 382–393.
[2] R. Xie, L. Zhang, H. Xu, Y. Zhong, X. Sui, Z. Mao, Construction of up-converting fluorescent carbon quantum dots/$Bi_{20}TiO_{32}$ composites with enhanced photocatalytic properties under visible light, Chem. Eng. J. 310 (2017) 79–90.
[3] A. Barati, M. Shamsipur, E. Arkan, L. Hosseinzadeh, H. Abdollahi, Synthesis of biocompatible and highly photoluminescent nitrogen doped carbon dots from lime: analytical applications and optimization using response surface methodology, Mater Sci Eng C Mater Biol Appl 47 (2015) 325–332.
[4] Q.Q. Dou, X. Fang, S. Jiang, L.C. Pei, T.C. Lee, J.L. Xian, Multi-functional fluorescent carbon dots with antibacterial and gene delivery properties, RSC Adv. 5 (2015) 46817–46822.
[5] J. Li, G. Zuo, X. Qi, W. Wei, X. Pan, T. Su, J. Zhang, W. Dong, Selective determination of Ag^{+} using Salecan derived nitrogen doped carbon dots as a fluorescent probe, Mater Sci Eng C Mater Biol Appl 77 (2017) 508–512.
[6] P.G. Luo, S. Sahu, S.-T. Yang, S.K. Sonkar, J. Wang, H. Wang, G.E. LeCroy, L. Cao, Y.-P. Sun, Carbon "quantum" dots for optical bioimaging, J. Mater. Chem. B 1 (2013) 2116.
[7] W.F. Zhang, H. Zhu, S.F. Yu, H.Y. Yang, Observation of lasing emission from carbon nanodots in organic solvents, Adv. Mater. 24 (2012) 2263–2267.
[8] F. Zhang, X. Feng, Y. Zhang, L. Yan, Y. Yang, X. Liu, Photoluminescent carbon quantum dots as a directly film-forming phosphor towards white LEDs, Nano 8 (2016) 8618–8632.
[9] H. Yu, R. Shi, Y. Zhao, G.I. Waterhouse, L.Z. Wu, C.H. Tung, T. Zhang, Smart utilization of carbon dots in semiconductor photocatalysis, Adv. Mater. 28 (2016) 9454–9477.
[10] Y. Li, Y. Hu, Y. Zhao, G. Shi, L. Deng, Y. Hou, L. Qu, An electrochemical avenue to green-luminescent graphene quantum dots as potential electron-acceptors for photovoltaics, Adv. Mater. 23 (2011) 776–780.
[11] X. Xu, R. Ray, Y. Gu, H.J. Ploehn, L. Gearheart, K. Raker, W.A. Scrivens, Electrophoretic analysis and purification of fluorescent single-walled carbon nanotube fragments, J. Am. Chem. Soc. 126 (2004) 12736–12737.
[12] A.B. Bourlinos, A. Stassinopoulos, D. Anglos, R. Zboril, V. Georgakilas, E.P. Giannelis, Photoluminescent carbogenic dots, Chem. Mater. 20 (2008) 4539–4541.
[13] Y.P. Sun, B. Zhou, Y. Lin, W. Wang, K.A. Fernando, P. Pathak, M.J. Meziani, B.A. Harruff, X. Wang, H. Wang, Quantum-sized carbon dots for bright and colorful photoluminescence, J. Am. Chem. Soc. 128 (2006) 7756–7757.
[14] L. Bao, Z.L. Zhang, Z.Q. Tian, L. Zhang, C. Liu, Y. Lin, B. Qi, D.W. Pang, Electrochemical tuning of luminescent carbon nanodots: from preparation to luminescence mechanism, Adv. Mater. 23 (2011) 5801–5806.
[15] Y. Dong, N. Zhou, X. Lin, L. Jianpeng, Y. Chi, G. Chen, Extraction of electrochemiluminescent oxidized carbon quantum dots from activated carbon, Chem. Mater. 22 (2010) 5895–5899.
[16] A.K. Samantara, S. Maji, A. Ghosh, B. Bag, R. Dash, B.K. Jena, Good's buffer derived highly emissive carbon quantum dots: excellent biocompatible anticancer drug carrier, J. Mater. Chem. B 4 (2016) 2412–2420.
[17] S. Qu, X. Wang, Q. Lu, X. Liu, L. Wang, A biocompatible fluorescent ink based on water-soluble luminescent carbon nanodots, Angew. Chem. Int. Ed. Eng. 51 (2012) 12215–12218.
[18] J. Wang, C.F. Wang, S. Chen, Amphiphilic egg-derived carbon dots: rapid plasma fabrication, pyrolysis process, and multicolor printing patterns, Angew. Chem. 51 (2012) 9297–9301.
[19] Q. Dou, J. Lu, K. Dan, C. Owh, J.L. Xian, Bioimaging and biodetection assisted with TTA-UC materials, Drug Discov. Today (2017) (DOI).
[20] S.S. Liow, H. Zhou, S. Sugiarto, S. Guo, M.L.S. Chalasani, N.K. Verma, J. Xu, J.L. Xian, Highly efficient supramolecular aggregation-induced emission-active pseudorotaxane luminogen for functional bioimaging, Biomacromolecules (2017) (DOI).
[21] S.S. Liow, Q. Dou, D. Kai, Z. Li, S. Sugiarto, C.Y.Y. Yu, R.T.K. Kwok, X. Chen, Y.L. Wu, S.T. Ong, Drug delivery: long-term real-time in vivo drug release monitoring with AIE thermogelling polymer (Small 7/2017), Small 13 (2016) 1603404.
[22] C. Zheng, H. Gao, D.P. Yang, M. Liu, H. Cheng, Y.L. Wu, J.L. Xian, PCL-based thermo-gelling polymers for in vivo delivery of chemotherapeutics to tumors, Mater. Sci. Eng. C 74 (2017) 110–116.
[23] V.P.N. Nguyen, N. Kuo, J.L. Xian, New biocompatible thermogelling copolymers containing ethylene-butylene segments exhibiting very low gelation concentrations, Soft Matter 7 (2011) 2150–2159.
[24] Y. Zhang, C.-F. Wang, L. Chen, S. Chen, A.J. Ryan, Microfluidic-spinning-directed microreactors toward generation of multiple nanocrystals loaded anisotropic fluorescent microfibers, Adv. Funct. Mater. 25 (2015) 7253–7262.
[25] A.M. Nightingale, J.C. de Mello, Microscale synthesis of quantum dots, J. Mater. Chem. 20 (2010) 8454.
[26] K. Hameed, Synthesis of ZnSe quantum dots using a continuous-flow microreactor and their white emission through energy transfer, ECS Solid State Lett. 2 (2013) R27–R30.
[27] C. Wiles, P. Watts, Recent advances in micro reaction technology, Chem. Commun. 47 (2011) 6512–6535.
[28] M. Krivec, K. Zagar, L. Suhadolnik, M. Ceh, G. Drazic, Highly efficient TiO_2-based microreactor for photocatalytic applications, ACS Appl. Mater. Interfaces 5 (2013) 9088–9094.
[29] P.W. Dunne, C.L. Starkey, M. Gimeno-Fabra, E.H. Lester, The rapid size- and shape-controlled continuous hydrothermal synthesis of metal sulphide nanomaterials, Nano 6 (2014) 2406–2418.
[30] J. Pan, A.O. El-Ballouli, L. Rollny, O. Voznyy, V.M. Burlakov, A. Goriely, E.H. Sargent, O.M. Bakr, Automated synthesis of photovoltaic-quality colloidal quantum dots using separate nucleation and growth stages, ACS Nano 7 (2013) 10158–10166.
[31] S. Yao, Y. Shu, Y.J. Yang, X. Yu, D.W. Pang, Z.L. Zhang, Picoliter droplets developed as microreactors for ultrafast synthesis of multi-color water-soluble CdTe quantum dots, Chem. Commun. (Camb.) 49 (2013) 7114–7116.
[32] Z.-H. Tian, J.-H. Xu, Y.-J. Wang, G.-S. Luo, Microfluidic synthesis of monodispersed

CdSe quantum dots nanocrystals by using mixed fatty amines as ligands, Chem. Eng. J. 285 (2016) 20–26.
[33] Y. Lu, L. Zhang, H. Lin, The use of a microreactor for rapid screening of the reaction conditions and investigation of the photoluminescence mechanism of carbon dots, Chemistry 20 (2014) 4246–4250.
[34] Z. Wang, B. Fu, S. Zou, B. Duan, C. Chang, B. Yang, X. Zhou, L. Zhang, Facile construction of carbon dots via acid catalytic hydrothermal method and their application for target imaging of cancer cells, Nano Res. 9 (2016) 214–223.
[35] G. Eda, Y.Y. Lin, C. Mattevi, H. Yamaguchi, H.A. Chen, I.S. Chen, C.W. Chen, M. Chhowalla, Blue photoluminescence from chemically derived graphene oxide, Adv. Mater. 22 (2010) 505–509.
[36] L. Cao, M.J. Meziani, S. Sahu, Y.P. Sun, Photoluminescence properties of graphene versus other carbon nanomaterials, Acc. Chem. Res. 46 (2013) 171–180.
[37] W. Cai, R.D. Piner, F.J. Stadermann, S. Park, M.A. Shaibat, Y. Ishii, D. Yang, A. Velamakanni, S.J. An, M. Stoller, Synthesis and solid-state NMR structural characterization of 13C-labeled graphite oxide, Science 321 (2008) 1815–1817.
[38] M.J. Krysmann, A. Kelarakis, P. Dallas, E.P. Giannelis, Formation mechanism of carbogenic nanoparticles with dual photoluminescence emission, J. Am. Chem. Soc. 134 (2012) 747–750.
[39] X. Zhai, P. Zhang, C. Liu, T. Bai, W. Li, L. Dai, W. Liu, Highly luminescent carbon nanodots by microwave-assisted pyrolysis, Chem. Commun. 48 (2012) 7955–7957.
[40] R.J. Fan, Q. Sun, L. Zhang, Y. Zhang, A.H. Lu, Photoluminescent carbon dots directly derived from polyethylene glycol and their application for cellular imaging, Carbon 71 (2014) 87–93.
[41] S.N. Baker, G.A. Baker, Luminescent carbon nanodots: emergent nanolights, Angew. Chem. Int. Ed. Eng. 49 (2010) 6726–6744.
[42] W. Kwon, G. Lee, S. Do, T. Joo, S.W. Rhee, Size-controlled soft-template synthesis of carbon nanodots toward versatile photoactive materials, Small 10 (2014) 506–513.
[43] H. Ding, S.B. Yu, J.S. Wei, H.M. Xiong, Full-color light-emitting carbon dots with a surface-state-controlled luminescence mechanism, ACS Nano 10 (2016) 484–491.
[44] Q. Dan, Z. Min, L. Zhang, H. Zhao, Z. Xie, X. Jing, R.E. Haddad, H. Fan, Z. Sun, CORRIGENDUM: formation mechanism and optimization of highly luminescent N-doped graphene quantum dots, Sci Rep 5 (2014) 7998.
[45] S. Zhu, Y. Song, X. Zhao, J. Shao, J. Zhang, B. Yang, The photoluminescence mechanism in carbon dots (graphene quantum dots, carbon nanodots, and polymer dots): current state and future perspective, Nano Res. 8 (2015) 355–381.
[46] T. Lai, E. Zheng, L. Chen, X. Wang, L. Kong, C. You, Y. Ruan, X. Weng, Hybrid carbon source for producing nitrogen-doped polymer nanodots: one-pot hydrothermal synthesis, fluorescence enhancement and highly selective detection of Fe (III), Nano 5 (2013) 8015–8021.
[47] Z. Zhang, Y. Pan, Y. Fang, L. Zhang, J. Chen, C. Yi, Tuning photoluminescence and surface properties of carbon nanodots for chemical sensing, Nano 8 (2016) 500–507.
[48] S. Zhu, Q. Meng, L. Wang, J. Zhang, Y. Song, H. Jin, K. Zhang, H. Sun, H. Wang, B. Yang, Highly photoluminescent carbon dots for multicolor patterning, sensors, and bioimaging, Angew. Chem. Int. Ed. Eng. 52 (2013) 3953–3957.
[49] Y. Dong, H. Pang, H.B. Yang, C. Guo, J. Shao, Y. Chi, C.M. Li, T. Yu, Carbon-based dots co-doped with nitrogen and sulfur for high quantum yield and excitation-independent emission, Angew. Chem. 52 (2013) 7800–7804.
[50] Y. Guo, Z. Wang, H. Shao, X. Jiang, Hydrothermal synthesis of highly fluorescent carbon nanoparticles from sodium citrate and their use for the detection of mercury ions, Carbon 52 (2013) 583–589.
[51] H. Žabov, aacute, V. Církva, M. Hájek, Microwave synthesis of fluorescent carbon nanoparticles with electrochemiluminescence properties, Chem. Commun. 103 (2009) 887–896.
[52] W. Wei, C. Xu, L. Wu, J. Wang, J. Ren, X. Qu, Non-enzymatic-browning-reaction: a versatile route for production of nitrogen-doped carbon dots with tunable multicolor luminescent display, Sci Rep 4 (2014) 3564.
[53] H. Li, X. He, Y. Liu, H. Huang, S. Lian, S.-T. Lee, Z. Kang, One-step ultrasonic synthesis of water-soluble carbon nanoparticles with excellent photoluminescent properties, Carbon 49 (2011) 605–609.
[54] M. Zheng, Z. Xie, D. Qu, D. Li, P. Du, X. Jing, Z. Sun, On off on fluorescent carbon dot nanosensor for recognition of chromium(VI) and ascorbic acid based on the inner filter effect, ACS Appl. Mater. Interfaces 5 (2013) 13242–13247.
[55] Y. Song, S. Zhu, S. Xiang, X. Zhao, J. Zhang, H. Zhang, Y. Fu, B. Yang, Investigation into the fluorescence quenching behaviors and applications of carbon dots, Nano 6 (2014) 4676–4682.
[56] P. Zhang, Z. Xue, D. Luo, W. Yu, Z. Guo, T. Wang, Dual-peak electrogenerated chemiluminescence of carbon dots for iron ions detection, Anal. Chem. 86 (2014) 5620–5623.
[57] W. Zhu, J. Zhang, Z. Jiang, W. Wang, X. Liu, High-quality carbon dots: synthesis, peroxidase-like activity and their application in the detection of H_2O_2, Ag^+ and Fe^{3+}, RSC Adv. 4 (2014) 17387–17392.
[58] M. Zhou, Z. Zhou, A. Gong, Y. Zhang, Q. Li, Synthesis of highly photoluminescent carbon dots via citric acid and Tris for iron(III) ions sensors and bioimaging, Talanta 143 (2015) 107–113.
[59] J. Yu, C. Xu, Z. Tian, Y. Lin, Z. Shi, Facilely synthesized N-doped carbon quantum dots with high fluorescent yield for sensing Fe^{3+}, New J. Chem. 40 (2016) 2083–2088.
[60] L. Zhou, J. Geng, B. Liu, Graphene quantum dots from polycyclic aromatic hydrocarbon for bioimaging and sensing of Fe^{3+} and hydrogen peroxide, Part. Part. Syst. Charact. 30 (2013) 1086–1092.
[61] H. Zhang, Y. Chen, M. Liang, L. Xu, S. Qi, H. Chen, X. Chen, Solid-phase synthesis of highly fluorescent nitrogen-doped carbon dots for sensitive and selective probing ferric ions in living cells, Anal. Chem. 86 (2014) 9846–9852.